

# The state of globular clusters at birth: emergence from the gas-embedded phase

Nathan Leigh<sup>1</sup>, Mirek Giersz<sup>2</sup>, Jeremy J. Webb<sup>3</sup>, Arkadiusz Hypki<sup>2</sup>, Guido De Marchi<sup>1</sup>, Pavel Kroupa<sup>4</sup>, Alison Sills<sup>3</sup> \*

<sup>1</sup>European Space Agency, Space Science Department, Keplerlaan 1, 2200 AG Noordwijk, The Netherlands

<sup>2</sup>Nicolaus Copernicus Astronomical Centre, Polish Academy of Sciences, ul. Bartycka 18, 00-716 Warsaw, Poland

<sup>3</sup>McMaster University, Department of Physics and Astronomy, 1280 Main St. W., Hamilton, Ontario, Canada, L8S 4M1

<sup>4</sup>Helmholtz-Institut für Strahlen- und Kernphysik, Nussallee 14-16, D-53115 Bonn, Germany

10 November 2021

## ABSTRACT

In this paper, we discuss the origin of the observed correlation between cluster concentration  $c$  and present-day mass function (PDMF) slope  $\alpha$  reported by De Marchi, Paresce & Pulone. This relation can either be reproduced from universal initial conditions combined with some dynamical mechanism(s) that alter(s) the cluster structure and mass function over time, or it must arise early on in the cluster lifetime, such as during the gas-embedded phase of cluster formation. Using a combination of Monte Carlo and  $N$ -body models for globular cluster evolution performed with the MOCCA and NBODY6 codes, respectively, we explore a number of dynamical mechanisms that could affect the observed relation.

For the range of initial conditions considered here, our results are consistent with an universal initial binary fraction  $\approx 10\%$  (which does not, however, preclude 100%) and an universal initial stellar mass function resembling the standard Kroupa distribution. *Most of the dispersion observed in the  $c$ - $\alpha$  relation can be attributed to two-body relaxation and Galactic tides. However, dynamical processes alone could not have reproduced the dispersion in concentration, and we require at least some correlation between the initial concentration and the total cluster mass.* We argue that the origin of this trend could be connected to the gas-embedded phase of cluster evolution.

**Key words:** globular clusters: general – celestial mechanics – stars: formation – methods: numerical – methods: N-body simulations – Galaxy: kinematics and dynamics.

## 1 INTRODUCTION

De Marchi, Paresce & Pulone (2007) showed that Milky Way (MW) globular clusters (GCs) exhibit a correlation between the logarithmic ratio of their tidal  $r_t$  and core  $r_c$  radii, called the concentration parameter  $c = \log(r_t/r_c)$ , and the slope of the low-mass stellar global mass function (MF)  $\alpha$ . That is, high concentration clusters tend to have steep MFs, while low concentration clusters tend to have flat MFs. The authors posited that this goes against the naive expectation that it is solely two-body relaxation that drives the evolution of both the concentration and the MF slope. In particular,

two-body relaxation causes the preferential evaporation of low-mass stars across the tidal boundary, while at the same time driving clusters toward a state of higher central density (e.g. Spitzer 1987; Heggie & Hut 2003). It follows that more concentrated clusters should be more severely depleted of preferentially low-mass stars and have a shallower MF than low-concentration clusters. This is precisely the opposite of what was found by De Marchi, Paresce & Pulone (2007) for a sample of 20 MW GCs. Clearly, the observed correlation between concentration and MF slope is puzzling.

Several authors have suggested mechanisms to explain this curious trend. De Marchi, Paresce & Pulone (2007) offered that GCs severely depleted of their low-mass stars underwent core collapse some time in the past, and have since recovered a normal radial density profile. However, this cannot explain the high concentrations observed in very massive clusters. Alternatively, Marks, Kroupa & Baumgardt

\* E-mail: nleigh@rssd.esa.int (NL); mig@camk.edu.pl (MG); webbjj@univmail.cis.mcmaster.ca (JW); ahycki@camk.edu.pl (AH); gdemarchi@rssd.esa.int (GD); pavel@astro.uni-bonn.de (PK); asills@mcmaster.ca (AS)

(2008) suggested that the observed correlation could be due to residual gas expulsion from initially mass segregated clusters, combined with the effects of unresolved binaries. The authors argued that extreme gas expulsion could produce clusters with low central densities, and hence low concentrations, and flat PDMFs at the low-mass end. Studying the interplay between the stellar initial mass function (IMF), concentration, and gas retention plays a crucial role in understanding the origins of star clusters in the Milky Way. For example, this approach leads to constraints on the sequence of events during the early evolution of the proto-Galaxy (Marks & Kroupa 2010), on the variation of the IMF in star bursts (Marks et al. 2012) and on the initial mass-radius relation of star clusters (Murray 2009; Marks & Kroupa 2012), and on the observed distribution of GC metallicities (Marks & Kroupa 2010).

Leigh et al. (2012) showed that the cluster-to-cluster variations observed in the PDMFs of MW GCs are consistent with what is expected if GCs were born with a universal initial mass function (IMF), and two-body relaxation is the dominant physical process driving the evolution of the MF. In other words, the power-law index of the central MF  $\alpha$  increases (i.e. the MF flattens) smoothly with decreasing cluster mass. This is what is expected from two-body relaxation, since it segregates low-mass stars to the outskirts where they escape from the cluster across the tidal boundary, and it operates with a rate that increases with decreasing cluster mass. This suggests that whatever mechanism is responsible for the observed correlation between  $c$  and  $\alpha$ , it should have primarily affected the cluster concentration relative to what is expected from two-body relaxation alone, as opposed to the slope of the MF  $\alpha$ . Said another way, if two-body relaxation is the only mechanism driving the internal evolution of clusters, then the expected dependence of  $\alpha$  on the total cluster mass is roughly consistent with what is observed.<sup>1</sup> This is not the case for the cluster concentration, however.

Other observational correlations have been reported for MW GCs, some of which are arguably also consistent with the general picture that GCs were born with approximately universal initial conditions and evolved via dynamics to their present-day forms. For example, Milone et al. (2012) recently performed a detailed study of the properties of main-sequence binaries in a sample of 59 GCs. The authors confirmed a previously reported (Sollima et al. 2007) anti-correlation between the binary fraction and the total cluster mass. Sollima (2008) showed via analytic methods that such an anti-correlation can arise naturally assuming an universal initial binary fraction that is independent of cluster mass. This can be explained by the disruption of binaries in the cluster core, combined with the evaporation of single stars from the cluster outskirts (e.g. Fregeau, Ivanova & Rasio 2009). The efficiency of the former should increase with increasing cluster density (Marks, Kroupa & Oh 2011) and hence mass, whereas the efficiency of the latter is driven by two-body relaxation and should increase with decreasing cluster mass. This contributes to high binary fractions

in low-mass clusters, and low binary fractions in high-mass clusters. Notwithstanding, Sollima (2008) cautioned that, based on existing observations of binary fractions in Galactic GCs, the data is also consistent with significant variations among the initial binary properties. This would, however, contradict the well-motivated universality hypothesis (Kroupa 2011).

In this paper, we argue that the origin of the observed distribution of concentration parameters  $c$  in GCs must be connected to the gas-embedded phase of cluster formation. The alternative is that globular clusters emerged from the embedded phase with universal initial conditions, and evolved via dynamics to their presently observed MFs and structural parameters. We perform a suite of numerical simulations for comparison to the observed  $c$ - $\alpha$  relation, varying the initial conditions in each model in order to identify those that yield the best agreement with the observations at the present-day cluster age. We also compare the simulated distribution of binary fractions as a function of the total cluster luminosity to the observed relation of Milone et al. (2012) in an effort to constrain to first-order the universality of the initial binary fraction in GCs.

We begin by considering in Section 2 different initial conditions that could affect the evolution of the MF slope and/or the concentration parameter. In Section 3, we describe the specific initial conditions we consider, as well as the Monte Carlo and  $N$ -body models used to simulate the cluster evolution. We present our results in Section 4 and, based on these results, we argue in Section 5 that dynamics alone could not have reproduced the observed  $c - \alpha$  relation. This implies that the observed relation must have originated very early on in the cluster lifetime, when gas was still present in significant quantities. Hence, we discuss the various mechanisms that could have contributed to the observed distribution of concentration parameters during the gas-embedded phase, and constrain the necessary conditions. We conclude in Section 6.

## 2 DYNAMICAL MECHANISMS AFFECTING THE $c$ - $\alpha$ RELATION

In this section, we consider several different dynamical mechanisms that could affect the evolution of the MF slope and/or the cluster concentration. We further describe the initial conditions for which each of these mechanisms should contribute to the observed  $c$ - $\alpha$  relation.

### 2.1 Binary stars

#### 2.1.1 Soft binaries

Soft binaries are characterized by their orbital energy, which must have an absolute value that is less than the average single star kinetic energy. This inequality gives (Heggie 1975):

$$a_{\text{soft}} > \frac{G\bar{m}}{\sigma^2}, \quad (1)$$

where  $a_{\text{soft}}$  denotes the semi-major axis of a soft binary,  $\bar{m}$  is the average stellar mass, and  $\sigma$  is the velocity dispersion. If a soft binary experiences a direct encounter with a single star, the total energy of such an encounter is positive, and the binary will likely be disrupted. Thus, on average, the

<sup>1</sup> This assumes that all clusters were born with similar initial mass functions, and is based on the central stellar MF, which is relatively insensitive to the effects of Galactic tides.

disruption of a soft binary by a single star serves to reduce the interloper’s speed, and hence kinetic energy.

If enough soft binaries are disrupted, this could affect the distribution of stellar velocities in a cluster. The cooling of a cluster through binary star disruption was first demonstrated by Kroupa, Petr & McCaughrean (1999). More recently, Fregeau, Ivanova & Rasio (2009) showed that the initial energy in soft binaries can be up to 10% of the total mechanical energy of a cluster. The authors argued that this is a sufficiently significant energy sink to drive a typical MW GC to core collapse. The disruption of soft binaries also causes a decrease in the binary fraction, not only due to the destruction of binaries but also due to the increase in single stars. This sudden increase in the number of single stars further contributes to increasing the relaxation time by increasing the total number of objects and decreasing the average object mass. Having said that, most soft binaries are disrupted very early on in the cluster lifetime, when massive stars are still present. The stellar evolution-driven mass loss from massive stars contributes to heating the core, causing the core radius to expand. The question is: does this tend to outweigh the energy sink provided by soft binaries, so that their disruption only serves to slow the expansion of the core?

The semi-major axis corresponding to the hard-soft boundary decreases with increasing cluster mass, since the velocity dispersion increases with increasing cluster mass (see Equation 1). Thus, assuming an universal initial binary fraction that is independent of the cluster mass, more massive clusters have more soft binaries initially (Kroupa 1995; Marks, Kroupa & Oh 2011). It follows that the efficiency of soft binary disruption as an energy sink should increase with increasing cluster mass. In other words, for a universal initial binary fraction and orbital parameter distributions, the disruption of soft binaries should contribute to a correlation between the total cluster mass and the concentration parameter, as observed.

### 2.1.2 Hard binaries

Hard binaries, for which the absolute value of the orbital energy exceeds the average kinetic energy of a single star, can also influence the central concentration via “binary burning” (e.g. Fregeau, Ivanova & Rasio 2009). In this case, the central density is sufficiently high that even very close binaries, for which the collisional cross-section is small, frequently undergo dynamical interactions with single stars. Here, the binary imparts additional kinetic energy to the escaping single star, becoming even harder in the process (Heggie 1975). Thus, hard binaries can act as heat sources in clusters with sufficiently high central densities, slowing and even reversing the tendency toward core collapse (e.g. Heggie & Hut 2003).

For a given binary fraction, low-mass clusters should contain the largest number of hard binaries, since the hard-soft boundaries in these clusters correspond to large orbital separations. Hence, core expansion driven by hard binary burning should also contribute to a correlation between the cluster mass and concentration. Fregeau, Ivanova & Rasio (2009) argued that most Milky Way GCs have not yet reached sufficiently high central densities to enter the binary burning phase of evolution, although the authors assumed that the concentration was lower in the past and that it has

been increasing steadily over time. Clusters with very high initial concentrations, on the other hand, are more likely to undergo binary burning early on, and this can contribute to decreasing the concentration parameter (Heggie & Giersz 2008, 2009).

## 2.2 Cluster expansion in a tidal field

Star clusters expand self-similarly in a tidal field (Gieles, Heggie & Zhao 2011). This contributes to decreasing the concentration parameter or, more accurately, reducing the rate at which the concentration increases due to two-body relaxation. This effect occurs in clusters that are initially tidally under-filling, since they have room to expand and experience a long delay before losing mass across the tidal boundary. Once a cluster fills its tidal radius, it experiences a steady increase in its concentration as the core radius shrinks due to two-body relaxation.

Assuming a universal distribution of initial cluster sizes, it is the most massive clusters that should expand the most in an under-filled tidal field, since they have the largest tidal radii. A useful, albeit simplistic (Webb, Sills & Harris 2012; Webb et al. 2013), approximation for the tidal radius is (von Hoerner 1957):

$$r_t = R_{GC} \left( \frac{M_{clus}}{M_g} \right)^{1/3}, \quad (2)$$

where  $R_{GC}$  is the Galactocentric distance of the cluster assuming a circular orbit,  $M_{clus}$  is the cluster mass, and  $M_g$  is the mass of the Galaxy, which here we assume to be a point mass.

Two-body relaxation acts to move lower mass stars outward to the cluster outskirts, where they preferentially escape across the tidal boundary. A cluster that experiences a stronger tidal field will undergo a more rapid stripping of its low-mass stars, due to the deeper potential in which the cluster sits and also the fact that a stronger tidal field translates into a smaller tidal radius. As the cluster loses mass, the process is accelerated, since the tidal radius decreases and the rate of two-body relaxation increases. For clusters with small Galactocentric distances, this can even result in an inversion of the mass function, so that its slope changes sign (Vesperini & Heggie 1997; Baumgardt & Makino 2003).

Tidal heating acts only on clusters with eccentric orbits, since a non-static tidal field implies that the depth of the gravitational potential is periodic, and additional energy is deposited within the stellar population with each perigalactic pass. This accelerates the rate of escape of preferentially low-mass stars across the tidal boundary. This is because low-mass stars in the outskirts have the lowest binding energies, so the additional energy accelerates these stars to speeds that exceed the escape velocity, at which point they have a positive total energy and become unbound. Overall, the net effect of tidal heating is to accelerate stars, causing an expansion of the cluster and its more rapid dissolution. Importantly, the mean mass loss per unit time due to external perturbations from the Galaxy are independent of cluster mass (Gieles et al. 2006; Gieles, Athanassoula & Portegies Zwart 2007). Thus, tidal heating should contribute to the observed dependence of mass function slope on concentration, since, for a given orbit, it should produce more

extended clusters with shallower MF slopes for smaller initial cluster masses, in agreement with the observations.

### 2.3 Initial stellar and remnant mass functions

The initial mass function can affect the evolution of the cluster structure in a number of ways. For example, for a given cluster mass, the initial mass function determines both the total number of stars and the average stellar mass, and hence the rate of two-body relaxation. Mass loss due to stellar evolution tends to cause clusters to expand (e.g. Chernoff & Weinberg 1990). Thus, clusters with a top-heavy initial mass function should expand more due to stellar evolution than clusters with a bottom-heavy initial mass function, since the former includes a larger fraction of massive stars. A top-heavy IMF should also generate more stellar remnants early on in the cluster lifetime, since the stellar lifetime decreases with increasing stellar mass.

Stellar remnants, including white dwarfs, neutron stars and black holes, represent an unseen component of globular clusters. Assuming a standard initial mass function (Kroupa 2002), they could constitute a substantial fraction of the total cluster mass at an age of  $\approx 12$  Gyr (e.g. Leigh et al. 2013). More importantly, remnants make up a much larger fraction of the *core* mass, since they are primarily confined to the central cluster region. This is because, at the time of their formation, stellar remnants descend from the most massive stars in the cluster, which have typically migrated into the core via mass segregation by the time of their death, if they did not form there in the first place. Even in very massive clusters for which the rate of two-body relaxation and hence mass segregation is slower, remnants that do not form in the core will still quickly migrate there via two-body relaxation since, after a few hundred Myr, they are the most massive objects in the cluster.

Given that they represent a significant, but unseen, mass component within the core, stellar remnants can have an important bearing on the concentration parameter. In particular, remnants should act as an additional heat source within the core, and we expect this to contribute to an increase in the core radius, and hence a decrease in the concentration parameter (e.g. Mackey et al. 2007, 2008; Sippel & Hurley 2013).

Stellar remnants could contribute (weakly) to the observed  $c$ - $\alpha$  relation. This is because, for a larger cluster mass, more massive stars are more likely to be selected from random sampling, and there is evidence that the maximum IMF mass increases with increasing cluster mass (Kroupa et al. 2013). More massive stars implies more massive remnants, which are more effective at heating the core, and hence lowering the concentration. It follows that, for a given IMF, stellar remnants could be more effective heat sources in more massive clusters, contributing to an anti-correlation between the cluster mass and concentration. Thus, although the data are consistent with a universal IMF in Milky Way globular clusters (e.g. De Marchi, Paresce & Portegies Zwart 2010; Paust et al. 2010; Kroupa et al. 2013; Leigh et al. 2012), the stellar IMF could compete against the observed  $c$ - $\alpha$  relation indirectly via stellar remnants. We do not expect this effect to typically be significant, however, given its stochastic nature, as reflected in the construction of the IMF via random sampling.

One interesting example that depends sensitively on the initial stellar and remnant mass functions involves the formation of an intermediate-mass black hole (IMBH). An IMBH can form from the runaway collisions of massive stars very early on in the cluster lifetime (Portegies Zwart et al. 2004). The IMBH can then continue to grow via subsequent mergers, and even gas accretion mediated by binary star evolution. If an IMBH forms, its presence should contribute to increasing the core radius, and hence decreasing the concentration parameter, by accelerating stars in its immediate vicinity (e.g. Lützgendorf et al. 2011). If IMBHs in GCs follow a similar scaling law as super-massive black holes (SMBHs) in galactic nuclei (Lützgendorf et al. 2013; Kruijssen & Lützgendorf 2013), then we would expect more massive clusters to harbour more massive IMBHs. In this case, IMBHs would contribute to a trend in which the concentration parameter decreases with increasing cluster mass, in clear disagreement with the observations.

## 3 MODELS

In this section, we describe the Monte Carlo and  $N$ -body codes used to simulate the cluster evolution, and list the initial conditions we consider. We use the Monte Carlo code MOCCA to simulate the majority of our model clusters, given its fast and robust coverage of the relevant parameter space. The agreement between MOCCA and  $N$ -body models is excellent for the case of static Galactic tides (Giersz et al. 2013), however MOCCA cannot treat non-static tides. Thus, we use the  $N$ -body code NBODY6 to quantify the impact of Galactic tides on the observed  $c$  -  $\alpha$  relation, since it incorporates a realistic treatment of the Galactic potential.

### 3.1 Monte Carlo models: MOCCA

We use the MOCCA code to produce the majority of our simulated clusters. It combines the Monte Carlo technique for cluster evolution with the *Fewbody* code (Fregeau et al. 2004) to perform numerical scattering experiments of small-number gravitational interactions, and relies on the Binary Stellar Evolution (BSE) code to track both stellar and binary evolution (Hurley, Pols & Tout 2000, 2002).

The MOCCA code offers several advantages, in particular the fast computation times required to run the simulations to completion. It also allows us to simulate clusters in regions of parameter space that are intractable with  $N$ -body codes. Specifically, since it relies on Monte Carlo methods, it can simulate realistic globular clusters composed of more than a million stars, and it can do so for 12+ Gyr of cluster evolution on time-scales of hours in real-time.<sup>2</sup> For more

<sup>2</sup> The MOCCA simulations are performed on a PSK2 cluster at the Nicolaus Copernicus Astronomical Centre in Poland. Each simulation is run on one CPU. The cluster is based on AMD (Advanced Micro Devices, Inc.) Opteron processors with 64-bit architecture (2-2.4 GHz). For 12+ Gyr of GC evolution, simulations with  $5 \times 10^4$  stars typically take  $\sim 1$  hour to complete, those with  $3 \times 10^5$  stars take 10-16 hours, and those with  $1.8 \times 10^6$  stars take 120-160 hours. The precise simulation run-time depends on the choice of initial conditions.

detailed information about the MOCCA code, see Hypki & Giersz (2013) and Giersz et al. (2013).

### 3.1.1 Initial conditions

We assume a King density profile with initial concentration  $W_0 = 6$ . Our clusters are not mass segregated to begin with, and all models are initially tidally under-filling. The degree of under-filling is set by the parameter  $f_{\text{und}} = r_t/r_h$ , where  $r_t$  and  $r_h$  are the tidal and half-mass radii, respectively. To put this parameter into context, a King model (King 1966) with  $W_0 = 6$  has a ratio between the tidal and half-mass radii of  $f_{\text{und}} = 6.79$ . We adopt a metallicity of  $Z = 0.001$  for all models.

The initial conditions we consider are shown in Table 1. We vary the initial mass function, binary fraction, kick velocities for NSs and BHs upon formation, the initial-final mass relation for BHs, the total number of stars, the ratio  $r_t/r_h$ , and the cluster age. We run models having a total of  $5 \times 10^4$ ,  $10^5$ ,  $2 \times 10^5$ ,  $3 \times 10^5$  or  $1.8 \times 10^6$  stars initially. For the  $N = 5 \times 10^4$  and  $N = 3 \times 10^5$  cases, we also re-run identical models with the same initial conditions but different random number seeds to assess fluctuations in the final cluster state that are intrinsic to the Monte Carlo method adopted by MOCCA. Snapshots are taken at 10, 11 and 12 Gyr for all models (unless indicated otherwise).

We adopt two different IMFs, both in the form:

$$\frac{dN}{dm} = m^{-\alpha}. \quad (3)$$

The first IMF we refer to as a standard Kroupa IMF (labeled *imf1* in Table 1), as taken from Kroupa, Tout & Gilmore (1993) in the mass range 0.08 - 100  $M_\odot$ . The second IMF is a two-segment Kroupa IMF (*imf2*), as taken from Kroupa (2008) with a single break mass at 0.5  $M_\odot$ , and low- and high-mass slopes of +1.3 and +2.3, respectively. In addition, we consider a modified IMF (*imf3*; instead of the two-segment Kroupa IMF) for the  $N = 100000$  and  $N = 200000$  cases, with a break mass at 0.85  $M_\odot$  and low- and high-mass slopes of +1.1 and +2.5, respectively.

For our standard model, the initial mass function adopted for the binaries is taken from Equation 1 of Kroupa, Gilmore & Tout (1991) in the mass range 0.08 to 100  $M_\odot$ , sampled with random pairing. We assume different initial binary fractions of 10%, 30%, 70% and 95%, along with different maximum orbital separations of 100 AU, 200 AU and 400 AU. The binary semi-major axis distribution is uniform in the logarithmic scale from  $2(R_1+R_2)$  to 100 AU (for the standard model). The binary eccentricities follow a modified thermal distribution taken from Equation 1 of Hurley et al. (2005). We also perform simulations with the initial binary orbital parameter distributions provided in Equation 4.46 of Kroupa et al. (2013), which are derived from empirical data (labeled *Kroupa13* in Table 1), in order to quantify the degree to which our assumptions for the initial binary orbital parameter distributions could affect our results.

Analytic formulae for stellar evolution are taken from Hurley, Pols & Tout (2000), and binary evolution is performed with the BSE code (Hurley, Pols & Tout 2002). We adopt two different initial-final mass relations for BHs. The first uses the initial-final mass relation from Hurley, Pols & Tout (2000) assuming no mass fallback, and the second is

the same but with mass fallback switched on (Belczynski, Kalogera & Bulik 2002). With mass fallback switched off, we adopt either a kick velocity of 265 km/s for both NSs and BHs (*kick1*), or we adopt 0 km/s for BHs and 265 km/s for NSs (*kick2*). With mass fallback switched on, both the BH mass and kick velocity depend on the progenitor mass.

### 3.2 N-body models: NBODY6

We use the NBODY6 direct  $N$ -body code (Aarseth 2003) to evolve a series of model clusters to an age of 12 Gyr. We list here only those model assumptions directly relevant to the tidal field, and refer the reader to Webb et al. (2013) for more specific details regarding the input parameters (e.g. metallicity, binary orbital distributions, etc.). Every  $N$ -body model begins with 96000 stars and 4000 binaries (i.e. an initial binary fraction of 4%)<sup>3</sup>, a total initial mass of  $6 \times 10^4 M_\odot$  and a half-mass radius of 6 pc, but follows a different orbit through the Galaxy. In particular, only the initial velocity changes between models, giving rise to different orbits within the Galactic potential.

To study the effect of a non-static tidal field, we simulate model clusters with orbital eccentricities of 0.5 and 0.9, each with a perigalactic distance of 6 kpc. To help quantify any differences between static and non-static tidal fields, we also simulate clusters with circular orbits at the perigalacticon and apogalacticon of each eccentric model. This produces models with circular orbits at 6 kpc, 18 kpc, and 104 kpc. Note that model names are based on orbital eccentricity (e.g. *e09*), and the distance at apogalacticon (e.g. *r104*).

The initial conditions for our  $N$ -body models have been summarized in Table 2. In the column labeled "Model", we distinguish between simulations corresponding to different orbits by providing the eccentricity ( $e$ ), and either the orbital semi-major axis ( $R_c$ ) if the orbit is circular or the perigalacticon distance ( $R_p$ ) if the orbit is eccentric.

The clusters follow orbits within a Galactic potential modeled by a  $1.5 \times 10^{10} M_\odot$  point-mass bulge, a  $5 \times 10^{10} M_\odot$  Miyamoto & Nagai (1975) disk (with  $a = 4.5$  kpc and  $b = 0.5$  kpc), and a logarithmic halo potential (Xue et al. 2008), as described in Aarseth (2003) and Praagman, Hurley & Power (2010). The combined mass profiles of all three components give rise to a circular velocity of 220 km/s at a galactocentric distance of 8.5 kpc. All clusters are made to orbit within the plane of the disk to eliminate the effects of tidal heating due to a non-spherically symmetric field and disc shocking.

## 4 RESULTS

In this section, we present the results of our simulations for globular cluster evolution. We begin by comparing the results of all simulations to the observed distributions of concentration, MF slope, binary fraction, and integrated V-band cluster magnitude. This is done to assess the overall

<sup>3</sup> We use the  $N$ -body models to quantify the effects of Galactic tides only. Hence, for our purposes, the results are approximately insensitive to the initial binary fraction, which is the same in all models.

**Table 1.** Initial conditions for all Monte Carlo (MOCCA) models.

Total Number of Stars	Time (in Gyr)	$r_t$ (in pc)	$f_{\text{und}}$	Binary Fraction	$a_{\text{max}}$ (in AU)	Model	Symbol				
1800000	10, 11, 12	125.33	60	10	100	standard (imf1 + kick1 + fallback)	5 pt. solid black triangle				
						no fallback	5 pt. solid blue triangle				
						imf2	5 pt. solid red triangle				
						standard	5 pt. solid black square				
						no fallback	5 pt. solid blue square				
						imf2	5 pt. solid red square				
			75	kick2	5 pt. solid green square						
				no fallback + imf2	5 pt. solid magenta square						
				kick2 + imf2	5 pt. solid cyan square						
				Kroupa13	5 pt. blue cross						
				300000	10, 11, 12	69.0	35	10	100	standard	4 pt. solid black triangle
										no fallback	4 pt. solid blue triangle
imf2	4 pt. solid red triangle										
binary mass segregation	5 pt. black cross										
standard	1 pt. open black square										
standard	3 pt. open black square										
30	standard	5 pt. open black square									
	70	standard	1 pt. open blue triangle								
		100	standard				1 pt. open blue square				
			400				standard	5 pt. open blue square			
							95	standard	1 pt. open green square		
								100	standard	3 pt. open green square	
200				standard	5 pt. open green square						
	400			standard	4 pt. solid black square						
		10		no fallback	4 pt. solid blue square						
			imf2	4 pt. solid red square							
			kick2	4 pt. solid green square							
			no fallback + imf2	4 pt. solid magenta square							
kick2 + imf2			4 pt. solid green square								
65	standard		4 pt. solid black pentagon								
	no fallback	4 pt. solid blue pentagon									
	imf2	4 pt. solid red pentagon									
	100	standard	4 pt. solid black hexagon								
		no fallback	4 pt. solid blue hexagon								
		imf2	4 pt. solid red hexagon								
		135	standard	4 pt. solid black heptagon							
			no fallback	4 pt. solid blue heptagon							
			imf2	4 pt. solid red heptagon							
	50		Kroupa13	4 pt. blue cross							
			10	standard	3 pt. solid black triangle						
				no fallback	3 pt. solid blue triangle						
imf3		3 pt. solid red triangle									
20		standard		3 pt. solid black square							
		no fallback		3 pt. solid blue square							
	imf3	3 pt. solid red square									
	10	Kroupa13	3 pt. blue cross								
		10	standard	2 pt. solid black triangle							
			no fallback	2 pt. solid blue triangle							
imf3			2 pt. solid red triangle								
20			standard	2 pt. solid black square							
			no fallback	2 pt. solid blue square							
	imf3		2 pt. solid red square								
	50000	10, 11, 12	37.96	20	10	100	standard	1 pt. solid black triangle			
							no fallback	1 pt. solid blue triangle			
							imf2	1 pt. solid red triangle			
25							standard	1 pt. solid black square			
							no fallback	1 pt. solid blue square			
							imf2	1 pt. solid red square			
	kick2	1 pt. solid green square									
	no fallback + imf2	1 pt. solid magenta square									
	kick2 + imf2	1 pt. solid cyan square									
30	standard	1 pt. solid black pentagon									
	no fallback	1 pt. solid blue pentagon									
	imf2	1 pt. solid red triangle									
	25	Kroupa13	1 pt. blue cross								

**Table 2.** Initial conditions for all  $N$ -body (NBODY6) models.

Total Number of Stars	Time (in Gyrs)	$r_t$ (in pc)	$f_{und}$	Model	Symbol
100000	12	40	6.7	$e = 0 + R_c = 6$	solid black line
100000	12	40	6.7	$e = 0.5 + R_p = 6$	solid blue line
100000	12	90	15.0	$e = 0 + R_c = 18$	solid red line
100000	12	40	6.7	$e = 0.9 + R_p = 6$	solid green line
100000	12	120	20.0	$e = 0 + R_c = 104$	solid magenta line

agreement between our models and the observations. Next, we quantify the degree to which each of the dynamical mechanisms listed in the previous section could have contributed to the observed  $c$ - $\alpha$  relation.

In order for the comparisons to be meaningful, it is crucially important that the simulated cluster properties are calculated analogously to the observed values. In other words, it is necessary to “observe” the simulated clusters in the same way as was done for the observations. *For the remainder of this paper, we calculate the concentration parameter using the cluster half-light radius instead of the tidal radius*, since the latter can be ambiguous, particularly in the models, resulting in an ambiguous definition of the concentration parameter (e.g. De Marchi, Paresce & Portegies Zwart 2010). We call this the *half-light concentration parameter*, denoted by  $c_h = \log(r_h/r_c)$ . Both the core and half-light radii are calculated from the 2-D surface brightness profiles of the models, and the core radius is defined as the distance from the cluster centre at which the surface brightness falls to half its central value.

We further ensure that the mass function slope and binary fraction are consistently calculated over the range of stellar masses (0.3 - 0.8  $M_\odot$ ) and binary mass ratios ( $q > 0.5$ ) used to derive the observed values. All  $f_b$  values refer to the *core* binary fractions. Finally, in analogy with the observed MFs, we consider binaries as unresolved single stars in the models when calculating the MF slope, with luminosities and colours determined by the combined light of the binary components (Kroupa, Gilmore & Tout 1991).

All models presented in this section were performed using the MOCCA code, with the exception of Section 4.2.2 for which only models performed using the NBODY6 code are presented.

#### 4.1 Comparisons to the observed distributions

We show the results for all Monte Carlo models in Figures 1 and 2 after 12 Gyr of cluster evolution, along with the observed values for comparison. Specifically, the *open red circles* show the observed values taken from De Marchi, Paresce & Pulone (2007), supplemented with additional global MF slopes taken from Paust et al. (2010) for those clusters not included in the study of De Marchi, Paresce & Pulone (2007). We do not show our model results after 10 and 11 Gyr of cluster evolution to avoid over-populating Figures 2 and 1. However, if all snapshots at 10, 11 and 12 Gyr are included, which somewhat reproduces the age spread in the Milky Way GC population, the agreement with the observed distributions is slightly better, and our over-arching conclusions are unaffected.

The first plot shows in the  $c_h - \alpha$  plane the observed

values of De Marchi, Paresce & Pulone (2007) with our simulated values, whereas the second shows in the  $M_V$ - $f_b$  plane the observed values of Milone et al. (2012) with our simulated values. Binary fractions apply only to the cluster core, and only to mass ratios  $q > 0.5$ . Integrated V-band magnitudes  $M_V$  are calculated from the final total cluster luminosity assuming  $M_{V,\odot} = 4.83$ .

For the *filled* symbols, the different colours correspond to different assumptions pertaining to the IMF and stellar remnants. In particular, the black, red, green, blue, cyan and magenta colours correspond to the standard IMF (imf1), modified Kroupa IMF (imf2), zero BH kick velocity (kick2), no BH fallback (no fallback), modified Kroupa IMF with zero BH kick (imf2+kick2) and modified Kroupa IMF with no BH fallback (imf2+no fallback) models, respectively.

In an effort to better communicate to the reader the results presented in Figures 1 and 2, we also systematically vary the size and shape of each symbol. For the filled points and crosses, the increasing point sizes correspond to increasing initial numbers of stars, with  $N = 50000$ ,  $N = 100000$ ,  $N = 200000$ ,  $N = 300000$  and  $N = 1800000$ . The initial ratio  $f_{und} = r_t/r_h$  also increases with increasing number of sides (i.e. triangle, square, pentagon, hexagon, etc.) for symbols of a given colour (see Table 1 for the exact  $f_{und}$  values).

The *filled* points correspond to models with an initial binary fraction of 10%. All *open* symbols (neglecting the red open circles) correspond to models with larger initial binary fractions. Specifically, the black, blue, and green open symbols correspond to initial binary fractions of 30%, 70% and 95%, respectively. All models corresponding to these open symbols adopt  $N = 300000$  stars initially and a standard Kroupa IMF (imf1). For these open symbols, the increasing point sizes correspond to increasing maximum binary orbital separations, where we consider the values  $a_{max} = 100$ , 200 and 400 AU. The black cross corresponds to a standard  $N = 300000$  model with an initial binary fraction of 10%, but with initial binary mass segregation imposed. Finally, the blue crosses (labeled Kroupa13 in Table 1) correspond to our standard model (imf1) with an initial binary fraction of 10%, but adopting the initial binary orbital parameter distributions of Kroupa et al. (2013).

##### 4.1.1 The observed $c_h - \alpha$ relation

Figure 1 shows that the simulated ranges in the concentration parameter and  $\alpha$  do not completely agree with the observations. Specifically, the models struggle to reproduce *both* low-concentration low- $\alpha$  clusters and high-concentration high- $\alpha$  clusters. Hence, if we increase (decrease) the initial concentration in all models, we will struggle to reproduce clusters with sufficiently low (high) con-

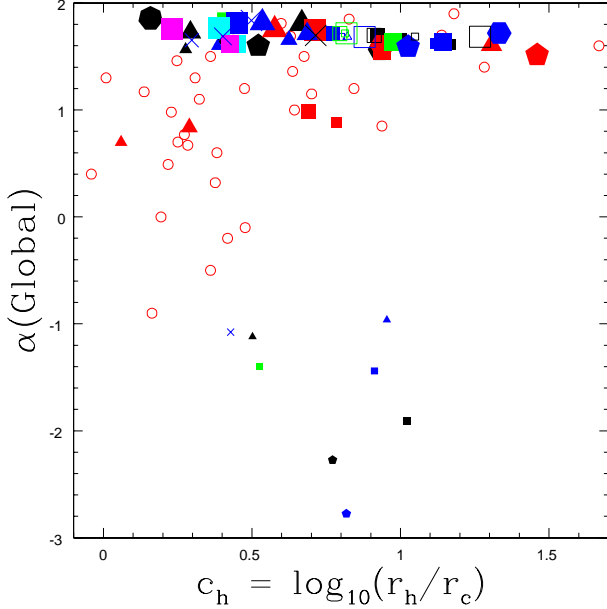


**Figure 1.** Results for all models in the  $c_h$ - $\alpha$ -plane at 12 Gyr, where  $\alpha$  is the power-law index of the MF over the mass range  $0.3 - 0.8 M_\odot$ . The half-light concentration is defined as  $c_h = \log(r_h/r_c)$ . A full description of each coloured symbol is provided in the text. The open red circles show the observed values taken from De Marchi, Paresce & Pulone (2007), supplemented with additional global MF slopes taken from Paust et al. (2010).

centrations without imposing additional assumptions (e.g. the formation of an IMBH). We struggle to reproduce sufficiently low- $\alpha$  values in low-concentration clusters in models that assume a standard Kroupa IMF (imf1), which is the case for most of our models. As illustrated by the solid red triangles and squares in Figure 1, the agreement appears better in models that assume a two-segment Kroupa IMF (imf2), and would be better still assuming an even more bottom-heavy IMF than considered in this paper.

As shown by the smallest points in Figure 1, there is a large gap in  $\alpha$  between the  $N = 50000$  models and the rest, with the  $N = 50000$  models also under-predicting  $\alpha$ . This can be corrected by adopting a slightly younger age for these clusters. However, most of the  $N = 50000$  models are approaching disruption at 12 Gyr, since they have lost a considerable fraction of their initial mass. Hence, the rate of escape of stars across the tidal boundary is high, as is the internal rate of two-body relaxation. At 11 Gyr, some of the  $N = 50000$  clusters have low- $\alpha$  values and low concentrations, in rough agreement with the observations. However, at 12 Gyr, all of these clusters have fully dissolved. Hence, this is a short-lived phase of the cluster evolution, lasting less than 1 Gyr. Consequently, it seems unlikely that *all* of the low- $\alpha$  low-concentration clusters observed in De Marchi, Paresce & Pulone (2007) are in the process of fully dissolving.

#### 4.1.2 The observed $M_V$ - $f_b$ relation

As is clear from Figure 2, the simulated ranges in both  $M_V$  and  $f_b$  are in excellent agreement with the observations for

the majority of our models. This suggests that our assumed range in the distribution of initial cluster masses is in reasonable agreement with that of the initial *cluster* mass function for the sample of Milone et al. (2012). Additionally, *for the assumed binary orbital parameter distributions adopted in this paper, the data are well-reproduced assuming an universal initial binary fraction of  $\approx 10\%$  in all clusters, independent of the cluster mass.* This is supported by the fact that models with initial binary fractions  $f_b = 30, 70$  and  $95\%$ , shown by the open squares in Figure 2, all over-predict the final binary fraction at the present cluster age. We obtain good agreement with the observations independent of whether or not we assume initial binary mass segregation (shown by the black cross in Figure 2).

Models that assume the initial binary orbital parameters distributions of Kroupa et al. (2013) and an initial binary fraction of  $10\%$ , shown by the blue crosses in Figure 2, yield final binary fractions that are lower than, but still comparable to, our other models and the observed values. This is because, for the initial cluster densities adopted in our models, a very large fraction of the initial binaries are soft, and are hence rapidly destroyed. This can be corrected by truncating the initial period distribution closer to the hard-soft boundary, so that a larger fraction of the initial binaries are hard, and hence more resilient to dynamical disruption. In this case, the distributions in Kroupa et al. (2013) would also yield good agreement to the observed binary fractions. Alternatively, the same result could be achieved by increasing the initial binary fraction, so that it is higher in denser clusters with hard-soft boundaries corresponding to very short orbital periods. In general, we are unable to rule out the possibility that other combinations of the initial binary fraction and orbital parameter distributions could also be consistent with the observations, such as the binary universality hypothesis described in Kroupa (2011). This will be the focus of a forthcoming paper.

## 4.2 The initial conditions

In this section, we describe how our results depend on each of the key assumptions that go into defining the initial conditions for our simulated clusters. We begin by quantifying in Figure 3 the efficiency of the various energy equipartition-driven mechanisms for cluster heating and cooling over the course of the cluster lifetime. We will refer to Figure 3 throughout the subsequent sub-sections, in which we consider these mechanisms individually in more detail, and how they affect the final half-light concentration parameter  $c_h$  and MF slope  $\alpha$ .

Figure 3 shows as a function of time the degree of cluster heating due to single-binary encounters (blue crosses), binary-binary encounters (red triangles) and stellar evolution-driven mass loss (black circles), as well as the degree of cooling due to single-binary encounters (cyan crosses), binary-binary encounters (magenta triangles) and direct stellar collisions (green circles). The MOCCA code divides model clusters into radial bins. Hence, the energy released/absorbed due to heating/cooling is calculated in each bin at each time-step, summed over the entire cluster, and divided by the total initial binding energy of the cluster (excluding the internal binding energy of binaries). Time-steps are taken at  $\sim 7.5$  Myr intervals. The energy



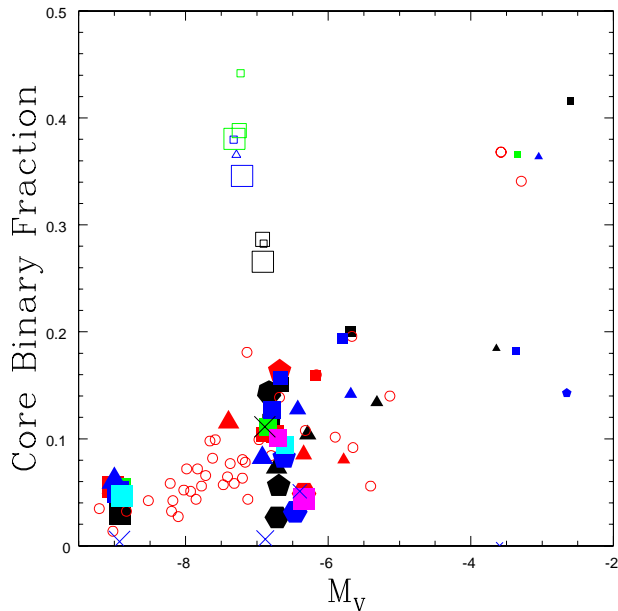


**Figure 2.** Results for all models in the  $M_V$ - $f_b$ -plane at 12 Gyr. The colour-coding as well as the properties (size and number of sides) of the data points are the same as in Figure 1. The open red circles show the observed values taken from Milone et al. (2012).

released/absorbed due to stellar evolution-driven mass loss is calculated from the change in potential energy, whereas the energy released/absorbed due to dynamical interactions is calculated directly from the Fewbody output.

As an example, consider the cyan crosses in Figure 3, which show the degree of cooling due to single-binary encounters. In the lower right panel, cooling due to single-binary interactions initially amount to  $\sim 10^{-6}$  of the total initial binding energy of the cluster. This increases with time to a level of  $\sim 10^{-2}$  of the initial cluster binding energy at  $\sim 1$  Gyr. The fractional energy absorbed due to single-binary encounters remains roughly constant (apart from a temporary dip at  $\sim 1$  Gyr) at  $\sim 10^{-3} - 10^{-2}$  for the next  $\sim 10$  Gyr. During this time, the long-period binary fraction is reduced due to disruption. It finally reduces to zero at  $\sim 11 - 12$  Gyr when all soft binaries have been disrupted. After this, single-binary encounters primarily serve to further harden close binaries, acting as a heat source by imparting energy to single stars (shown by the dark blue crosses in Figure 3).

In all models, stellar evolution (black squares) is the dominant heating mechanism early on in the cluster lifetime, when massive stars are still present in significant numbers. After several Gyr of cluster evolution, single-binary (dark blue crosses) and, to a lesser extent, binary-binary (red triangles) encounters take over as the dominant heating source. Early on in the cluster lifetime, however, both single-binary (cyan crosses) and binary-binary (magenta triangles) encounters act as an important source of cooling, since soft binaries are still present in significant numbers. Finally, direct stellar collisions (green circles) are never the dominant source of cooling, and tend to absorb energy at a much lower rate than the other heating/cooling mechanisms.

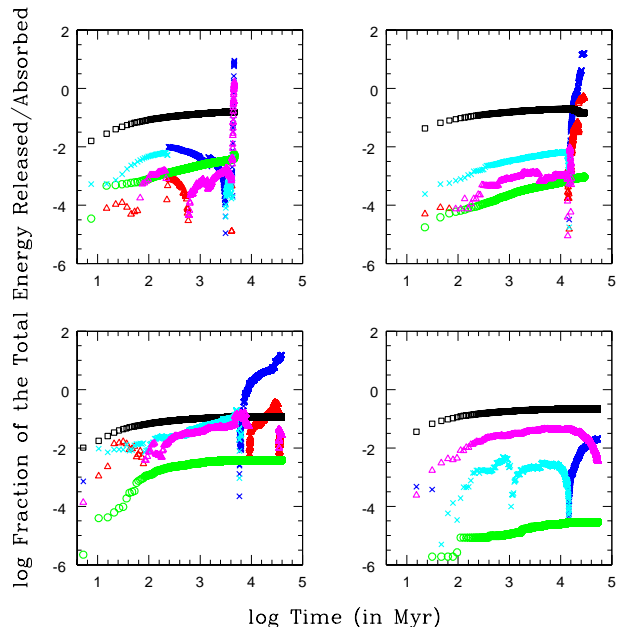


**Figure 3.** Heating and cooling as a function of time (in Myr) for a few selected models. On the y-axis, the fraction of the total initial binding energy of the cluster that is absorbed or released by each mechanism is plotted. The dark blue crosses, red triangles and black squares correspond to heating due to single-binary encounters, binary-binary encounters and stellar evolution, respectively. The cyan crosses, magenta triangles and green circles correspond to cooling due to single-binary encounters, binary-binary encounters and direct stellar collisions, respectively. Models shown in the top insets begin with  $N = 1800000$ ,  $f_b = 0.1$ ,  $a_{\max} = 100$  AU and either  $f_{\text{und}} = 60$  (right) or  $f_{\text{und}} = 125$  (left). The model shown in the bottom left inset begins with  $N = 300000$ ,  $f_b = 0.1$ ,  $a_{\max} = 100$  AU and  $f_{\text{und}} = 100$ . Finally, the model shown in the bottom right insets begins with  $N = 300000$ ,  $f_b = 0.95$ ,  $a_{\max} = 400$  AU and  $f_{\text{und}} = 35$ .

#### 4.2.1 Binaries

The disruption of soft binaries is only effective as a cooling mechanism for the first  $\sim$  few Gyr of cluster evolution. However, during this time, the cooling due to soft binary disruption is outweighed by heating due to stellar evolution-induced mass loss, since massive stars are still present in significant numbers. The heating caused by the mass loss from these massive stars contributes to an expansion of the core, and the energy sink provided by the disruption of soft binaries only serves to slow the mass loss-driven expansion of the core. This is shown in Figure 3. Cooling due to the disruption of soft binaries is shown by the cyan crosses and magenta triangles, whereas heating caused by stellar evolution-driven mass loss is shown by the black squares.

Clusters that begin with high initial binary fractions do not necessarily end up with high concentrations, independent of our assumption for the maximum orbital separation, and hence the fraction of soft binaries. The open squares in Figures 1 and 2 correspond to model clusters with high initial binary fractions. As is clear from Figure 1, all of these models end up with final core binary fractions that are much higher than observed. At the same time, Figure 1 shows that

these same clusters end up with final concentrations that are approximately independent of the initial binary fraction.

It seems unlikely that the disruption of soft binaries contributed significantly to the observed distribution of concentration parameters. In order for the disruption of soft binaries to have a significant effect on the core radius, and hence concentration, our results suggest that the period distribution would need to be heavily peaked just beyond the hard-soft boundary. In this case, most binaries would be soft, with orbital energies slightly larger than that corresponding to the hard-soft boundary. This would maximize the effectiveness of soft binary disruption as an energy sink, and would help to create massive clusters with high concentrations. However, we are unaware of a theoretical reason for why the period distribution should be heavily peaked near the hard-soft boundary, and this would conflict heavily with empirically-derived period distributions (Kroupa 1995; Kroupa & Petr-Gotzens 2011).

Binary burning becomes an effective heat source much later in the cluster lifetime, typically only after  $\sim 10$  Gyr of evolution (with the exception of the model shown in the upper left panel in Figure 3, which evolved to a high central density on a shorter time-scale than the other models). This is because, for most of the lifetime of a cluster, the concentration is increasing, and sufficiently high central densities are required in order for interactions between (primarily) single stars and binaries to occur at a fast enough rate for binary burning to become effective. In our models, binary burning mainly serves to slow the contraction of the core, as opposed to completely reversing the collapse and driving a re-expansion of the core. The effectiveness of binary burning is shown by the blue crosses and red triangles in Figure 3, which correspond to heating due to single-binary and binary-binary encounters, respectively.

#### 4.2.2 Galactic tides

In this section, we rely almost exclusively on the results of our  $N$ -body models to quantify the effects of Galactic tides on the observed  $c_h$ - $\alpha$  relation. These are presented in Figure 4, which shows the evolution in the  $c_h$ - $\alpha$ -plane for models with different orbits through the Galaxy but identical initial conditions (see Section 3.2 for the specific initial conditions). The black, blue, red, green, and magenta lines, in that order, correspond to orbits with decreasing average tidal fields. The main conclusion to be drawn from Figure 4 is that *Galactic tides typically have only a small effect on the evolution of the ratio  $c_h = r_h/r_c$ , but a large effect on the evolution of the global stellar MF*. Below, we explain the origin of this important result. We will refer back to Figure 4 throughout this section to help illustrate our results.

Galactic tides affect the evolution of the stellar MF in the following way. For a given cluster mass, clusters that experience the strongest tidal fields undergo the most rapid mass loss due to the fact that the tidal radius decreases with decreasing Galactocentric distance. Consequently, clusters exposed to stronger tidal fields undergo the most rapid flattening of their MFs (i.e. the greatest rate of decrease in  $\alpha$ ), since low-mass stars are preferentially accelerated to wider orbits within the cluster potential. This mass loss translates into a reduction in the time-scale for two-body relaxation. The shorter relaxation time exacerbates the trend, so that

more mass is lost from the cluster at an ever-increasing rate, shortening the relaxation time even further. Thus, on average, we expect clusters that experience the strongest tidal fields to undergo the most rapid flattening of their stellar MFs.

Galactic tides affect the evolution of the cluster concentration in the following way. There is an overall trend for clusters that experience the strongest tidal fields to have the smallest radii (Webb et al. 2013).<sup>4</sup> This trend sets in within roughly the first Gyr of evolution, and becomes exacerbated as the clusters continue to evolve. This is because clusters with small Galactocentric distances (and hence small tidal radii) have the least room to expand before filling their tidal radii. Once these clusters are tidally-filling, their core and half-mass radii begin to contract due to two-body relaxation (e.g. Spitzer 1987; Heggie & Hut 2003).

Despite the fact that all radii change considerably over the cluster evolution, the net effect of these changes is that the evolution in the concentration parameter is small when calculated using  $r_h$  instead of  $r_t$ , changing by a factor only slightly greater than unity. *Although  $r_c$  and  $r_h$  themselves change significantly, the ratio  $r_h/r_c$  remains roughly the same for all clusters*. This is clearly illustrated in Figure 4 for all simulated clusters, almost independent of their orbit through the Galaxy. That is, for model clusters with the same initial size and concentration the evolution in  $c_h$  appears to be orbit-independent in Figure 4, with  $c_h$  increasing from 0.8 to almost 1 after a Hubble time. Any differences are within the observational uncertainties. The only exception to this is initially tidally under-filling clusters on relatively circular orbits at large Galactocentric distances. In these clusters, the core radius decreases due to two-body relaxation at a noticeably faster rate than does the half-mass radius. This contributes to an increase in the concentration over time while  $\alpha$  remains more or less constant, albeit the effect remains small in our models, even for the most distant orbits (see below).

To better explore the effect that initially tidally under-filling clusters may have on the results of Figure 4, we make use of lower mass versions of our  $N$ -body models. These lower mass models contain 48000 single stars and 2000 binaries initially, and are described in detail in Webb et al. (2013). Due to their smaller masses, these models are less computationally expensive, which allows us to explore a range of initial half-mass radii. For clusters with initial half-mass radii of 2 pc and 4 pc, the central concentration increases while the cluster expands to fill its tidal radius (see Figure 7 in Webb et al. (2013)), and  $\alpha$  remains roughly constant. This results in tidally under-filling clusters evolving towards the high- $c_h$ , high- $\alpha$  region of Figure 1. Once the tidal radius is filled,  $\alpha$  decreases at a rate similar to that in the models shown in Figure 4, while maintaining a near constant half-mass concentration  $c_h$ . However, in *very* tidally under-filling clusters at large Galactocentric distances, 12 Gyr may not be enough time to enter this phase of evolution. Thus, although we are unable to reproduce the highest concentrations observed by De Marchi, Paresce & Pulone

<sup>4</sup> In this section, we always refer to the 3-D radii, instead of the observational values calculated from the surface brightness profiles.

(2007), initially very tidally under-filling clusters tend to produce the highest final concentrations.

These results suggest that Galactic tides should contribute to, and likely even dominate, the dispersion in the observed  $c_h - \alpha$  relation. Most of this dispersion should appear at the low-concentration (and typically low-mass) end of the distribution, since these include both initially massive, heavily stripped clusters at small Galactocentric distances and initially low-mass clusters at large Galactocentric distances that have lost only a small fraction of their mass. This can help to account for some of the dispersion in  $\alpha$  at the low- $c_h$  end not reproduced in our models, as seen in Figure 1.

More quantitatively, the smallest Galactocentric distance in the sample of De Marchi, Paresce & Pulone (2007) is  $\gtrsim 2.1$  kpc and  $\alpha$  does not evolve significantly at Galactocentric distances beyond  $\approx 100$  kpc. Hence, at the low-concentration end of the distribution, we estimate from Figure 4 that tides should contribute to a dispersion in  $\alpha$  of  $\delta\alpha \approx \pm(0.6 - 0.7)$  for a given initial cluster mass. This value of  $\delta\alpha$  is a minimum, since the clusters plotted in Figure 4 all began with the same initial total mass. Hence,  $\delta\alpha$  should be larger for a range of initial total cluster masses, as expected in the proto-Milky Way (e.g. Marks et al. 2012; Kroupa et al. 2013). For comparison, the presently observed range is  $\delta\alpha_{\text{obs}} \approx 3.0$  (from -1.0 up to 2.0). Given the range of initial cluster masses and Galactocentric distances that should apply to the sample of De Marchi, Paresce & Pulone (2007), we conclude that Galactic tides dominate the dispersion in the observed distribution of present-day MF slopes.

We note that tides contribute significantly to altering the *global* mass function, however the effect is much less pronounced for the central MF evaluated near the core (see Webb et al., in preparation). This is because the *central* MF is primarily altered via two-body relaxation-driven mass segregation, and is relatively insensitive to the escape of stars across the tidal boundary. This explains why the results presented in Leigh et al. (2012), which focused on the annulus immediately outside the core (between one and two core radii from the cluster centre), are consistent with the general picture that the cluster-to-cluster differences observed in the PDMFs of GCs arise from an universal IMF modified primarily by two-body relaxation-driven dynamical evolution. This general picture is also consistent with the results presented in this paper.

#### 4.2.3 The initial stellar and remnant mass functions

In Figure 5, we show how our results change upon varying both the initial stellar mass function and the initial-final mass relation for BHs. The black circles, red squares, and blue triangles correspond to snapshots at 10, 11 and 12 Gyr, respectively. In order of increasing size, the size of the points correspond to clusters with 50000, 100000, 200000, 300000 and 1800000 stars initially.

As illustrated by the black (10 Gyr), red (11 Gyr) and blue (12 Gyr) squares in Figure 5, the slope of the MF tends to decrease over time. Clusters with the lowest masses (i.e.  $N = 50000$ ; shown by the smallest point-size in Figure 5) end up with the smallest MF slopes, in qualitative agreement with the observations (e.g. Paust et al. 2010; Leigh et al. 2012). More quantitatively, Figure 1 shows that mod-

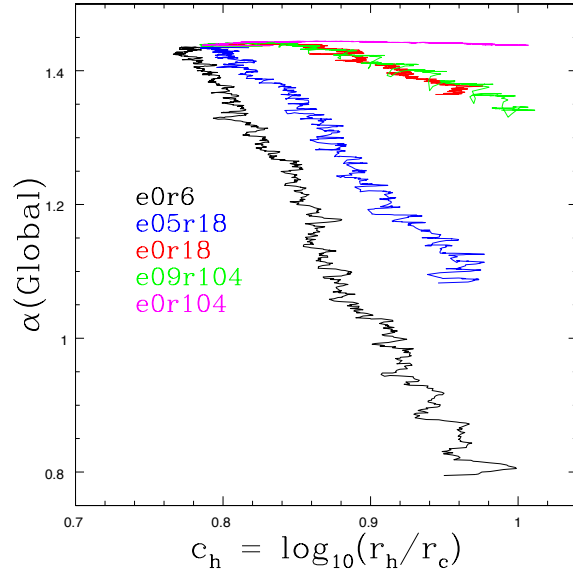


**Figure 4.** Evolution in the  $c_h - \alpha$  plane over 12 Gyr for each  $N$ -body model. All clusters begin with  $\alpha \approx +1.5$  and evolve toward slightly higher concentrations and lower MF slopes. Each model is colour-coded, such that model names are based on the distance at apogalacticon  $r_a$  (e.g. r104 for  $r_a = 104$  kpc), and the orbital eccentricity (e.g. e09 for  $e = 0.9$ ). Note that the observed trend (De Marchi, Paresce & Pulone 2007) is opposite to that evident here.

els that assume a standard Kroupa IMF struggle to reproduce clusters with sufficiently low- $\alpha$  and low-concentration, as was found by Zonoozi et al. (2011) for the GC Palomar 14. The agreement is slightly better in models that assume a non-standard IMF, as shown by the solid red triangles and squares in Figure 1. However, this is only because the non-standard IMF has more massive stars, which lose the most mass due to stellar evolution, and this contributes to an expansion of the core. Thus, the final concentration is smaller for a non-standard IMF due to the additional mass loss from massive stars very early on in the cluster evolution.

As mentioned, we confirm that the half-light concentration tends to increase over time, however this need not always be the case. For example, stellar evolution causes an expansion of the core very early on in the cluster lifetime, and the concentration can change from increasing to decreasing during the final stages of cluster dissolution. More importantly, *there is a stochasticity in the simulations such that nearly identical initial conditions can produce significantly different final evolutionary states for our model clusters.*

As illustrated in Figure 5, most of the stochasticity observed in our Monte Carlo simulations seems to be tied to the dynamical evolution of the remnant sub-population within

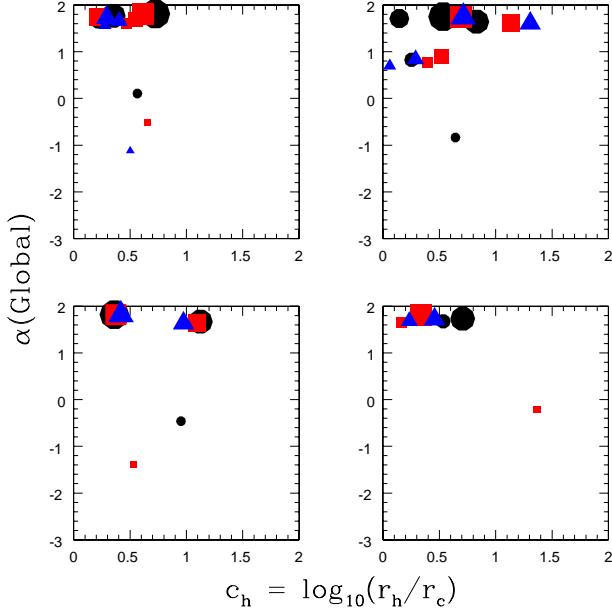


**Figure 5.** Results in the  $c_h - \alpha$ -plane for different IMFs and initial-final mass relations for BHs. We show the results for a normal Kroupa IMF (top left inset), as well as an IMF with a single break mass at  $0.5 M_\odot$  and low-mass and high-mass slopes of  $+1.3$  and  $+2.3$ , respectively (top right inset). We also try adjusting the amount of fallback onto BHs upon their formation. The no fallback case is shown in the bottom left inset. Finally, the bottom right inset shows our results assuming both a non-standard two-segment IMF and mass fallback onto BHs.

the cluster. For example, in some of our models, an IMBH forms through a new pathway not yet discussed in the literature (for more details, see Giersz, Leigh & Hypki 2013, in preparation). In this scenario, an IMBH forms from a single originally stellar-mass black hole that grows in mass due to dynamical interactions that induce mergers between the growing BH and (typically) other stellar remnants, combined with binary evolution-driven mass-transfer events. To initiate this process, one BH must be left in the system after all BH-forming supernovae have ceased, or a single BH must be formed via NS-NS or NS-WD mergers. The presence of additional BHs tends to prevent the formation of a single very massive BH due to competitive merging and accretion, followed by their dynamical ejection from the cluster. The process is facilitated by the fact that the growing BH is rarely isolated, since the time-scale for it to capture another object and form a binary is very short. The presence of such a binary companion is crucial, since it reduces the time-scale for dynamical interactions and hence mergers. In our standard models, the mass growth of the BH is typically slow and requires a few Gyr of cluster evolution before an IMBH forms. The final core radius is typically higher in these models than in those for which no IMBH forms.

Therefore, our results show that remnants can also contribute to the dispersion in the observed  $c$ - $\alpha$  relation. Based on the results shown in Figure 5, we estimate that remnants can contribute to a dispersion in  $c_h$  of up to  $\delta c_h \approx 1.0$ , and possibly more in a few rare cases.

## 5 DISCUSSION

In this section, we argue that stellar dynamics alone is not enough to reproduce the observed  $c_h - \alpha$  relation. While the effects of two-body relaxation combined with Galactic tides *can* reproduce the observed dispersion in  $\alpha$  (Leigh et al. 2012), we do not find a strong increase in the concentration parameter with increasing cluster mass, and hence increasing  $\alpha$  (e.g. De Marchi, Paresce & Portegies Zwart 2010; Leigh et al. 2012), in our models, regardless of the initial (universal) conditions and assumptions adopted. This implies that some other non-dynamical mechanism is also required to reproduce the observed distribution of concentration parameters. That is, the initial distribution of cluster concentrations cannot be universal when clusters begin evolving in relative isolation due solely to energy equipartition-driven dynamical evolution. Some other mechanism that is independent of the internal dynamical evolution of clusters is also required. We go on to explore the possibility that the origin of the observed  $c_h - \alpha$  relation is tied to the gas-embedded phase of cluster evolution.

### 5.1 Energy equipartition-driven dynamical evolution alone cannot reproduce the observed $c_h - \alpha$ relation

Based on our results, two-body relaxation-driven dynamical evolution alone cannot reproduce the observed  $c_h - \alpha$  relation. This is because our simulated clusters struggle to *simultaneously* produce both high-concentration high- $\alpha$  and low-concentration low- $\alpha$  clusters, provided we adopt the same empirically-motivated universal IMF for every cluster (Kroupa 2011; Kroupa et al. 2013). The problem is that, unlike the IMF, we do not have a reasonable empirically- or theoretically-motivated guess at what the initial concentration should be, as a function of any cluster parameter.

Shifting the initial mass function slope and/or distribution of concentrations in either direction will only worsen the agreement at the opposite end. For example, if we begin with clusters that are initially more concentrated, we will struggle even more to produce sufficiently low concentration clusters with flat MFs, and vice versa. However, in principle, it is possible to match the observed  $c_h - \alpha$  relation at the high- $c_h$  high- $\alpha$  end by assuming a higher initial concentration. Similarly, a lower initial concentration combined with a lower value for  $\alpha$  would improve the agreement at the low- $c_h$  low- $\alpha$  end.

For these reasons, it is difficult to constrain the exact spread in the initial distribution of concentration parameters required to explain the observed distribution. Instead, we re-iterate that the observed spread in  $\alpha$  *can* be reproduced from an universal IMF combined with energy equipartition-driven dynamical evolution (Leigh et al. 2012).<sup>5</sup> This quan-

<sup>5</sup> Although we have shown consistency with the universality hypothesis for the IMF, our results do not serve as a proof that the universality hypothesis is correct. Although variations in the IMF with the initial cluster mass (or other cluster properties) have not been ruled out in this study, any such dependences explored in future studies should be firmly rooted in star formation theory given that the observations are also in general consistent with the universality hypothesis for the IMF (e.g. Kroupa et al. 2013)

titatively reproduces the general trend that lower mass clusters tend to have shallower PDMFs (De Marchi, Paresce & Pulone 2007; De Marchi, Paresce & Portegies Zwart 2010; Paust et al. 2010). Meanwhile, the observed spread in  $c_h$  *cannot* be reproduced from an universal distribution of initial concentrations. Thus, some other mechanism that is independent of the internal dynamical evolution of clusters must also be operating in order to reproduce the (weak) trend that higher mass clusters (with, on average, steeper MFs) tend to have higher present-day concentrations (Harris 1996, 2010 update). In the subsequent sections, we explore different possibilities that could contribute to this observational trend, with a focus on the gas-embedded phase of cluster evolution.

### 5.1.1 Caveat: stellar collisions and tidal interactions

Milgrom & Shapiro (1978) argued that tidal dissipation during close fly-bys between single stars can reduce the stars' kinetic energies, and contribute to a contraction of the core on a shorter time-scale than is achieved by two-body relaxation alone. Similarly, direct collisions between single stars should also dissipate kinetic energy (Lightman & Shapiro 1977). The single-single collision rate increases with increasing cluster mass (Leonard 1989), so that the most massive clusters should experience the most efficient tidal dissipation due to close fly-bys and direct collisions between single stars. Thus, tidal interactions and collisions may both contribute to the observed  $c - \alpha$  relation, since they both contribute to a correlation between cluster mass and concentration.

A detailed treatment of the effects of collisions and tidal interactions is beyond the scope of this paper, however our results suggest that these effects can likely be ignored in future studies. As illustrated in Figure 3, the energy sink provided by collisions is never the dominant heating/cooling mechanism affecting the concentration. In fact, the effect is typically negligible, and remains approximately constant over the cluster lifetime for the central densities reached in our models. It follows that the energy sink offered by tidal interactions is also unlikely to ever be the dominant heating/cooling mechanism. This is because the rate of tidal capture events should be comparable to the rate of direct collisions, since the efficiency of tidal capture decreases rapidly with increasing distance of closest approach. Also, tidal interaction events that do not result in binary formation typically remove significantly less energy than tidal captures, since the energy dissipated due to tides quickly becomes negligible with increasing distance of closest approach.

## 5.2 The gas-embedded phase of cluster formation

In the previous section, we argued that it is unlikely that the observed  $c_h - \alpha$  relation has a purely energy equipartition-driven origin. It follows from this, and the assumption that the observed (central) MF distribution alone *can* be accounted for purely by two-body relaxation-driven dynamical evolution (e.g. Paust et al. 2010; Leigh et al. 2012), that the origin of the observed distribution of cluster concentrations must be tied to some other physical process(es). For example, hierarchical merging of clusters early on in their lifetimes could perhaps contribute. Alternatively, external

perturbations from the Galaxy may also play a role, such as disc shocking due to passages through the plane of the Galaxy or interactions with nearby giant molecular clouds or other star clusters. In this section we focus on the gas-embedded phase of cluster formation, and discuss some of the various mechanisms that could have operated when gas was still present in significant quantities.

### 5.2.1 Cluster expansion due to rapid gas expulsion

Marks, Kroupa & Baumgardt (2008) argue that rapid gas expulsion combined with primordial mass segregation can produce the observed low-concentration clusters with flat MFs. Clusters expand in response to the sudden removal of their gas. Although the tidal radius also increases due to the loss of mass, the central cluster regions expand more significantly, causing the concentration to decrease. At the same time, preferentially low-mass stars in the outskirts become unbound, and escape from the cluster. This simultaneously lowers the concentration and decreases the mass function slope, improving the agreement at the low- $c_h$  low- $\alpha$  end of the observed relation. The results presented in this paper suggest that an even more bottom-heavy IMF in the mass range  $0.3 - 0.8 M_\odot$  than assumed in our standard model (imf1), combined with a lower initial half-light concentration, could reproduce the observed  $c_h - \alpha$  relation at the low- $c_h$  end. Importantly, this would approximately reproduce the post-gas expulsion MF and cluster concentration described in Marks, Kroupa & Baumgardt (2008) and Marks et al. (2012). Disc shocking and external perturbations from other massive bodies on nearby orbits within the Galaxy could also contribute to this general trend. This is because these mechanisms should typically deposit additional energy within clusters, causing them to expand and accelerating the rate of escape of preferentially low-mass stars across the tidal boundary (e.g. Vesperini & Heggie 1997).

Marks, Kroupa & Baumgardt (2008) also caution that unresolved binaries can contribute to making the MF index  $\alpha$  appear smaller than it actually is. This is because each binary causes two single stars to disappear from the mass function, and an additional star with a derived mass higher than either binary component to be included. Hence, on average, binaries artificially deplete the low-mass end of the MF while simultaneously over-populating the high-mass end. Unresolved binaries should have at most a small effect on our results, however. This is because the simulated mass functions are derived by treating binaries as unresolved objects, in analogy with the observed mass functions. Additionally, in all but the lowest mass clusters considered here, the number of binaries is so few that they do not significantly affect the derived power-law index of the MF (e.g. Milone et al. 2012).

### 5.2.2 Cluster contraction due to prolonged gas retention

There now exists evidence that the most massive MW GCs underwent multiple episodes of star formation (e.g. Piotto et al. 2007). This trend does not appear in much lower mass open clusters, and even the lowest mass globulars (e.g. Gratton, Carretta & Bragaglia 2012). The currently favoured scenario to explain these multiple populations suggests that

either star formation was on-going for  $\approx 10^8$  years (e.g. Conroy & Spergel 2011), or massive clusters re-accreted gas from which new stars were formed (e.g. Pflamm-Altenburg & Kroupa 2009). This additional star formation indirectly implies that gas was present in these clusters for a prolonged period of time relative to their lower mass counterparts.

Several mechanisms could contribute to increasing the concentration during the gas-embedded phase. For example, the occurrence of star formation suggests relatively high gas accretion rates for the stars. Independent of whether or not the gas actually remains bound to the accretor, this could act to reduce the accretor velocities due to conservation of momentum. For this to be the case, all that is required is that the “accreted” gas be accelerated by the accretor such that the two are co-moving relative to the background medium (Hoyle & Lyttleton 1939; Bondi & Hoyle 1944; Bondi 1952). In general, accretion from the interstellar medium should both increase the central stellar density and accelerate the mass segregation process (Leigh et al. 2013), since the accretion rate typically increases with increasing accretor mass.

Active star formation also suggests high gas densities. Consequently, gas dynamical friction could be very efficient, since the gas dynamical friction force scales linearly with the gas density. The net effect of gas dynamical friction is to transfer kinetic energy from the stars to the surrounding gas, causing the central stellar density to increase but the central gas density to decrease. We note that the gas dynamical friction force also depends critically on whether or not the motion of the perturber relative to the gas is subsonic or supersonic. Given that stars are actively forming during much of the gas-embedded phase, this suggests that the gas must have been relatively cold. It follows that the sound-speed should have been small compared to the stellar velocity dispersion, and hence that the motion was predominantly supersonic. The most efficient gas drag occurs when the relative velocity is slightly less than the sound speed (Lee & Stahler 2011) (i.e. when the stellar and gas velocity dispersions are roughly equal), however previous work has also shown it to be effective in the supersonic regime (Dokuchaev 1964; Ruderman & Spiegel 1971; Rephaeli & Salpeter 1980; Ostriker 1999).

The increase in stellar density due to the presence of gas could result in positive feedback, and help to prolong the gas-embedded phase. This is because a higher stellar density translates into a deeper potential well, and hence a larger escape velocity. This could in turn imply a larger gas retention fraction and/or a longer gas expulsion time (e.g. Heggie & Giersz 2009).

If more massive clusters tend to have higher gas densities primordially, retain their gas for longer or re-accrete more gas from the surrounding intra-cluster medium than do low-mass clusters, this could contribute to a correlation between cluster mass and concentration. This is because, in this case, the efficiencies of both accretion from the ISM (onto stars) and gas dynamical friction should increase with increasing cluster mass.

We conclude that the gas-embedded phase of cluster evolution could be crucially important for the origin of the observed  $c_h - \alpha$  relation. This is not only due to the fact that the results presented in this paper suggest that two-body relaxation-driven dynamical evolution alone cannot explain

the observed distribution of concentrations, but also because the gas damping mechanisms we have considered should all contribute to the observed trend of increasing concentration with increasing cluster mass. More work will be needed to better isolate the origin of the observed  $c_h - \alpha$  relation and, in particular, the degree to which it was present at the end of the gas-embedded phase. Future studies with this goal should aim to constrain the gas-embedded phase of cluster evolution (e.g. central gas density, gas retention time, etc.) as a function of the total cluster mass.

## 6 SUMMARY

In this paper, we consider the origin of the correlation between cluster concentration and present-day mass function slope observed in the Milky Way globular cluster population. To this end, we generate a suite of Monte Carlo and  $N$ -body models using the MOCCA and NBODY6 codes, respectively, for star cluster evolution. We compare the results to the observed correlation between cluster concentration and mass function slope, as well as to the observed anti-correlation between cluster mass and binary fraction. These relations can either be reproduced from universal initial conditions combined with some dynamical mechanism(s) that alter(s) the distributions over time, or they must arise very early on in the cluster lifetime, such as during the gas-embedded phase of cluster formation. We explore a number of dynamical mechanisms that could contribute to, or even reproduce, the observed trends. Our key conclusions are:

- \* Galactic tides combined with energy equipartition-driven dynamical evolution can account for most, if not all, of the observed dispersion in the present-day MF slope  $\alpha$ , but not all of the dispersion in the concentration parameter  $c_h$ .
- \* Dynamical effects induced by stellar remnants should also contribute non-negligibly to the dispersion observed in  $c_h$ .
- \* Some other mechanism that is independent of the internal dynamical evolution of clusters must also operate in order to reproduce the observed dispersion in  $c_h$ .
- \* Whatever the mechanism(s) responsible, it should operate by preferentially increasing  $c_h$  in more massive clusters in order to reproduce the observed trend that clusters with steep MFs (and typically large total cluster masses) tend to have the highest concentrations.

Thus, we conclude that energy equipartition-driven dynamical evolution alone could not have reproduced the observed relation between concentration and mass function slope. Consequently, we suggest that this trend could be connected to the gas-embedded phase of cluster evolution. Specifically, we argue that cluster contraction due to prolonged gas retention could account for the most concentrated clusters with the steepest mass functions, and cluster expansion due to rapid gas expulsion could account for the least concentrated clusters with the flattest mass functions.

## ACKNOWLEDGMENTS

We would like to thank Michael Marks and Hagai Perets for useful discussions, as well as an anonymous referee whose suggestions helped to improve this manuscript. This work



was partly supported by the Polish Ministry of Science and Higher Education through the grant N N203 38036 and by the National Science Centre through the grants DEC-2012/07/B/ST9/04412 and DEC-2011/01/N/ST9/06000.

## REFERENCES

- Aarseth S., Hénon M., Wielen R. 1974, *A&A*, 37, 183
- Aarseth, S.J. 2003, *Gravitational N-body Simulations: Tools and Algorithms* (Cambridge Monographs on Mathematical Physics). Cambridge University Press, Cambridge
- Baumgardt H., Makino J. 2003, *MNRAS*, 340, 227
- Baumgardt H., De Marchi G., Kroupa P. 2008, *MNRAS*, *ApJ*, 685, 247
- Belczynski K., Kalogera V., Bulik T. 2002, *ApJ*, 572, 407
- Binney J., Tremaine S., 1987, *Galactic Dynamics* (Princeton: Princeton University Press)
- Bondi H., Hoyle F. 1944, *MNRAS*, 104, 273
- Bondi H. 1952, *MNRAS*, 112, 195
- Brodie J. P., Strader J. 2006, *ARA&A*, 44, 193
- Chernoff D. F., Weinberg M. D. 1990, *ApJ*, 351, 121
- Conroy C., Spergel D. N. 2011, *ApJ*, 726, 36
- De Marchi G., Paresce F., Pulone L. 2007, *ApJL*, 665, 65
- De Marchi G., Paresce F., Portegies Zwart S. 2010, *ApJ*, 715, 1
- De Marchi G., Paresce F., Pulone L. 2007, *ApJL*, 665, 65
- Dokuchaev V. P. 1964, *Sovet Astron.*, 8, 23
- Duquennoy A., Mayor M. 1991, *A&A*, 248, 485
- Fall S. M., Zhang Q. 2001, *ApJ*, 561, 751
- Fregeau J. M., Cheung P., Portegies Zwart S. F., Rasio F. A. 2004, *MNRAS*, 352, 1
- Fregeau J. M., Ivanova N., Rasio F. A. 2009, *ApJ*, 707, 1533
- Gieles M., Portegies Zwart S. F., Baumgardt H., Athanassoula E., Lamers H. J. G. L. M., Sipiør M., Leenaarts J. 2006, *MNRAS*, 371, 793
- Gieles M., Athanassoula E., Portegies Zwart S. F. 2007, *MNRAS*, 376, 809
- Gieles M., Heggie D. C., Zhao H. 2011, *MNRAS*, 413, 2509
- Giersz M., Heggie D. C., Hurley J. R., Hypki A. 2013, *MNRAS*, 431, 2148
- Gratton R., Carretta E., Bragaglia A. 2012, *Astronomy & Astrophysics Review*, in press (arXiv:1201.6526)
- Harris, W. E. 1996, *AJ*, 112, 1487 (2010 update)
- Harris G. L. H., Harris W. E. 2011, *MNRAS*, 410, 2347
- Heggie D. C., Hut P. 2003, *The Gravitational Million-Body Problem: A Multidisciplinary Approach to Star Cluster Dynamics* (Cambridge: Cambridge University Press)
- Heggie D. C. 1975, *MNRAS*, 173, 729
- Heggie D. C., Giersz M. 2008, *MNRAS*, 389, 1858
- Heggie D. C., Giersz M. 2009, *MNRAS*, 397, 46
- Hoyle F., Lyttleton R. A. 1939, in *Proceedings of the Cambridge Philosophical Society*, 35, 405
- Hurley J. R., Pols O. R., Tout C. A. 2000, *MNRAS*, 315, 543
- Hurley J. R., Pols O. R., Tout C. A. 2002, *MNRAS*, 329, 897
- Hurley J. R., Pols O. R., Aarseth S. J., Tout C. A. 2005, *MNRAS*, 363, 293
- Hurley, J.R. 2008a, *Cambridge N-body Lectures*, Lecture Notes in Physics, 760. Springer-Verlag, Berlin, p.283
- Hurley, J.R. 2008b, *Cambridge N-body Lectures*, Lecture Notes in Physics, 760. Springer-Verlag, Berlin, p.321
- Hypki A., Giersz M. 2013, *MNRAS*, 429, 1221
- King I. R. 1966, *AJ*, 71, 64
- Kravtsov A. V., Gnedin O. Y. 2005, *ApJ*, 623, 650
- Kroupa P., Gilmore G., Tout C. A. 1991, *MNRAS*, 251, 293
- Kroupa P., Tout C. A., Gilmore G. 1993, *MNRAS*, 262, 545
- Kroupa P. 1995, *MNRAS*, 277, 1507
- Kroupa P., Petr M. G., McCaughrean M. J. 1999, *New Astronomy*, 4, 495
- Kroupa P. 2002, *Science*, 295, 82
- Kroupa P. 2008, *Cambridge N-body Lectures*, Lecture Notes in Physics, 760. Springer-Verlag, Berlin, p. 181
- Kroupa P. 2011, *Proceeds of the International Astronomical Union*, IAU Symposium 270, 141-149
- Kroupa P. Petr-Gotzens M. G. 2011, *A&A*, 529, 92
- Kroupa P., Weidner C., Pflamm-Altenburg J., Thies I., Dabringhausen J., Marks M., Maschberger T. 2013, *Planets, Stars and Stellar Systems Vol. 5*, ed. Oswalt T. D. & Gilmore G. (Springer Science & Business Media Dordrecht: Dordrecht), 115-242
- Kruijssen J. M. D., Portegies Zwart S. F. 2009, *ApJL*, 698, L158
- Kruijssen J. M. D., Lützgendorf N. 2013, *MNRAS Letters*, accepted (arXiv:1306.0561)
- Lee A. T., Stahler S. W. 2011, *MNRAS*, 416, 3177
- Leigh N. W., Umbreit S., Sills A., Knigge C., De Marchi G., Glebbeek E., Sarajedini A. 2012, *MNRAS*, 422, 1592
- Leigh N. W., Böker T., Maccarone T. J., Perets H. B. 2013, *MNRAS*, 429, 2997
- Leonard P. J. T. 1989, *AJ*, 98, 217
- Lightman A. P., Shapiro S. L. 1977, *ApJ*, 213, 183
- Long K. S., Charles P. A., Dubus G., 2002, *ApJ*, 569, 204
- Lützgendorf N., Kissler-Patig M., Noyola E., Jalali B., de Zeeuw P. T., Gebhardt K., Baumgardt H. 2011, *A&A*, 533, 36
- Lützgendorf N., Kissler-Patig M., Neumayer N., Baumgardt H., Noyola E., de Zeeuw P. T., Gebhardt K., Jalali B., Feldmeier A. 2013, *A&A*, 555, 26
- Mackey A. D., Wilkinson M. I., Davies M. B., Gilmore G. F. 2007, *MNRAS*, 379L, 40
- Mackey A. D., Wilkinson M. I., Davies M. B., Gilmore G. F. 2008, *MNRAS*, 386, 65
- Maeder A. 2009, *Physics, Formation and Evolution of Rotating Stars*. Berlin: Springer-Verlag
- Marks M., Kroupa P., Baumgardt H. 2008, *MNRAS*, 386, 2047
- Marks M., Kroupa P. 2010, *MNRAS*, 406, 2000
- Marks M., Kroupa P., Oh S. 2011, *MNRAS*, 417, 1684
- Marks M., Kroupa P., Dabringhausen J., Pawlowski M. S. 2012, *MNRAS*, 422, 2246
- Marks M., Kroupa P. 2012, *A&A*, 543, 8
- Milgrom M., Shapiro S. L. 1978, *ApJ*, 223, 991
- Milone A. P., Piotto G., Bedin L. R., Aparicio A., Anderson J., Sarajedini A., Marino A. F., Moretti A., Davies M. B., Chaboyer B., Dotter A., Hempel M., Marin-Franch A., Majewski S., Paust N. E. Q., Reid I. N., Rosenberg A., Siegel M. 2012, *A&A*, 540, 16
- Miyamoto M., Nagai R. 1975, *PASJ*, 27, 533
- Murray N. 2009, *ApJ*, 691, 946

- Ostriker E. C. 1999, ApJ, 513, 252  
Paust N. E. Q., Reid I. N., Piotto G., et al. 2010, AJ, 139, 476  
Pflamm-Altenburg J., Kroupa P. 2009, ApJ, 706, 516  
Piotto G., Bedin L. R., Anderson J., King I. R., Cassisi S., Milone A. P., Villanova S., Pietrinferni A., Renzini A. 2007, ApJ, 661, L53  
Plummer H.C. 1911, MNRAS, 71, 460  
Portegies Zwart S. F., Baumgardt H., Hut P., Makino J., McMillan S. L. W. 2004, Nature, 428, 724  
Praagman A., Hurley J., Power C. 2010, New Astronomy, 15, 46  
Rephaeli Y., Salpeter E. E. 1980, ApJ, 240, 20  
Ruderman M. A., Spiegel E. A. 1971, ApJ, 165, 1  
Sippel A. C., Hurley J. R. 2013, MNRAS, 430, 30  
Sollima A., Beccari G., Ferraro F. R., Fusi Pecci F., Sarajedini A. 2007, MNRAS, 380, 781  
Sollima A. 2008, MNRAS, 388, 307  
Spitzer L. Jr. 1987, Dynamical Evolution of Globular Clusters (Princeton, NJ: Princeton Univ. Press)  
Tremaine S. D., Ostriker J. P., Spitzer L. Jr. 1975, ApJ, 196, 407  
Vesperini E., Heggie D. C. 1997, MNRAS, 289, 898  
von Hoerner S. 1957, ApJ, 125, 451  
Webb, J.J., Sills A., Harris, W. E. 2012, ApJ, 746, 93  
Webb, J.J., Harris W. E., Sills A., Hurley J. R. 2013, ApJ, 764, 124  
Xue X. X., et al. 2008, ApJ, 684, 1143  
Zhang Q., Fall S. M. 1999, ApJ, 527, 81  
Zonoozi A. H., Küpper A. H. W., Baumgardt H., Haghi H., Kroupa P., Hilker M. 2011, MNRAS, 411, 1989

This paper has been typeset from a  $\text{\LaTeX}$  file prepared by the author.